

Stereoscopic PIV measurements of flow over a riblet surface at high Reynolds number

Ozkan, G. M.; Elsinga, G. E.; Breugem, W. P.; Stübing, D.; Reynolds, K. J.; Westerweel, J.

DOI

[10.1016/j.expthermflusci.2020.110246](https://doi.org/10.1016/j.expthermflusci.2020.110246)

Publication date

2021

Document Version

Final published version

Published in

Experimental Thermal and Fluid Science

Citation (APA)

Ozkan, G. M., Elsinga, G. E., Breugem, W. P., Stübing, D., Reynolds, K. J., & Westerweel, J. (2021). Stereoscopic PIV measurements of flow over a riblet surface at high Reynolds number. *Experimental Thermal and Fluid Science*, 120, Article 110246. <https://doi.org/10.1016/j.expthermflusci.2020.110246>

Important note

To cite this publication, please use the final published version (if applicable). Please check the document version above.

Copyright

Other than for strictly personal use, it is not permitted to download, forward or distribute the text or part of it, without the consent of the author(s) and/or copyright holder(s), unless the work is under an open content license such as Creative Commons.

Takedown policy

Please contact us and provide details if you believe this document breaches copyrights. We will remove access to the work immediately and investigate your claim.



Stereoscopic PIV measurements of flow over a riblet surface at high Reynolds number



G.M. Ozkan^{a,*}, G.E. Elsinga^b, W.-P. Breugem^b, D. Stübing^c, K.J. Reynolds^d, J. Westerweel^b

^a Dep. of Mechanical Engineering, Çukurova University, 01330, Sarıcam, Adana, Turkey

^b Laboratory for Aero & Hydrodynamics, Process and Energy Department, Delft University of Technology, Mekelweg 2, 2628 CD Delft, the Netherlands

^c Fraunhofer Institute for Manufacturing Technology and Advanced Materials IFAM, Bremen, Germany

^d AkzoNobel/International Paint Ltd, Gateshead, UK

ARTICLE INFO

Keywords:

Turbulent boundary layer
Drag reduction
Riblet coating
Stereo-PIV

ABSTRACT

The effect of drag reducing riblets on the flow structure was examined experimentally for a turbulent boundary layer at $Re_\theta = 9890$ and riblet spacing $s^+ = 13.4$. Trapezoidal riblets were used, which were attached to the water tunnel wall as a coating. Force measurements were performed to quantify the amount of drag reduction. Then, the mechanism underlying this reduction was investigated by stereo-PIV measurements in the cross-stream plane. To determine the effect of the drag reducing riblets, the results were compared with the smooth flat plate. Time-averaged turbulent statistics such as turbulent kinetic energy and Reynolds shear stress were found to be lower over the riblets compared to the flat surface. Two-point correlations of the fluctuating velocity components were calculated to elucidate the average flow structure size and strength, where riblets significantly suppressed the turbulent structures. Quadrant analysis of the Reynolds shear stress was performed to assess the change in ejection and sweep events and the results were found to be in correspondence with previous works.

1. Introduction

The challenge of reducing skin friction has been quite attractive to scientists, since any decrease in drag would result in such substantial energy savings in modern technology and even a small amount of fuel savings can be crucially important for all kinds of vehicles in transportation. For instance, typically about half of the total drag of an aircraft at subsonic speeds is due to the skin friction, while it is up to 90% for underwater vehicles. Therefore, turbulent boundary layer theory and control techniques over surfaces have been studied intensively over the past decades. These studies were initiated by Prandtl [1] who is the inventor of boundary layer theory and the first researcher on boundary layer control. There is abundant experimental and numerical research showing a remarkable drag reduction on surfaces classified with active and passive methods [2,3]. Nature serves as a useful area for the inspiration of various flow control mechanisms, which is called “biomimetics”. The air and marine animals intrinsically use individual flow control techniques for their survival which could possess potential methods to be implemented on real engineering applications [4–6]. For example, the structure of dermal denticles, i.e., the tooth-like structure of shark skin can be mimicked by longitudinal grooves on a flat plate, called riblets. This surface modification was first

studied at NASA Langley Research Center [7] considering different shapes including rectangular, triangular (trapezoidal, sawtooth or v-groove) and scalloped geometries. Detailed numerical [8] and experimental [9] researches covering fairly large parameter ranges have revealed the effect of various riblet shapes on drag reduction. The experiments in an oil channel of Bechert et al. [9] reported up to 9.9% drag reduction for blade type riblets; however, even though the blade type gives the best efficiency, it is not easy to implement in practice as they are mechanically weak and easily break off the surface. Therefore the triangular riblets have been widely investigated [9–11] yielding 4–8% drag reduction and have been adapted to real engineering applications concerning aeronautics and marine industry.

The underlying mechanism of drag reduction by riblets has also been an important research topic in the scientific community. The main idea was that the riblets impede the cross-stream translation of the streamwise vortices in the viscous sublayer [12], which results in the attenuation of cross-stream velocity fluctuations by keeping the vortices above the riblet tips [13]. According to this physical explanation, although the surface area is larger for the riblet case, which might increase drag, the lower cross-stream fluctuations limit the generation of shear stress and momentum transfer near the wall. Therefore, the total drag acting on the riblet surface is reduced compared with the flat

* Corresponding author.

E-mail address: gmozkan@cu.edu.tr (G.M. Ozkan).

<https://doi.org/10.1016/j.expthermflusci.2020.110246>

Received 7 April 2020; Received in revised form 10 July 2020; Accepted 1 September 2020

Available online 12 September 2020

0894-1777/ © 2020 Elsevier Inc. All rights reserved.

surface. This claim has been supported by numerical research of Goldstein et al. [11] showing that the generated vortices formed on the surface remain above the riblet tips by creating a low-velocity channel in the riblet valleys. Then, this low velocity reduced the velocity gradient compared with flat surface, and hence the wall shear stress and the drag force. According to the mentioned studies, there are some transient secondary vortex formations inside the riblet valleys, although their contribution to drag is insignificant. Even though above physical explanations have been verified, drag reducing mechanism of the riblets is still under investigation by researchers using various modern techniques to obtain well-resolved structures within the flat plate boundary layer, especially at high Reynolds numbers. Through these, hot-wire anemometry measurements of Park and Wallace [14] close to the riblet valleys proved that vertical flux of streamwise momentum is significantly reduced resulting in diminished wall shear stress near the bottom of the riblet valley with a 4% drag reduction calculated by integrating wall shear stress over the riblets. Laser Doppler velocimetry (LDV) and hydrogen bubble flow visualization were used to observe the coherent structures in the near wall region [15]. Results revealed that the riblet surface enhances the thicknesses of viscous sublayer, buffer region and integral constant C in the log-law while reducing the low-speed streak spacing by 20% as an indication of lower drag. High-resolution PIV experiments [16] including limited data for viscous and buffer layers have revealed that the number distributions of the small-scale spanwise vortices were significantly decreased in the riblet surface and the turbulence intensity. Also, Reynolds stresses were reduced by the drag-reducing effect of the riblet grooves.

Recently, the actual denticles structure of sharkskin (from *Isurus oxyrinchus*) was compared with those of riblet surfaces in the turbulent boundary layer [17]. They reported that the actual sharkskin denticles are not able to reduce the high shear rates close to the surface which resulted in larger drag forces by 44–50% compared with the flat surface; however, 5% drag reduction was achieved by the use of riblets. Another study by planar, volumetric and long-range microscopic PTV [18] reported the reduction in turbulent fluctuations and attenuation of ejection and sweep motions close to the riblet surface as compared with the smooth wall.

In this research, a trapezoidal type riblet coating was investigated utilizing drag force and stereo-PIV measurements and analyzed for a further understanding of the relationship between drag reduction and flow dynamics. Force measurements were compared with the study of Benschop et al. [19] which includes Taylor- Couette measurements over the same riblets. The novelty of this research is that the coating has a realistic riblet dimension ($s = 92 \mu\text{m}$) required for actual flow conditions found in most industrial applications in which the Re_τ is on the order of 10^3 – 10^5 [20]. Furthermore, this research might be one of the rare PIV implementations performed in water at this high Reynolds number dealing with turbulent boundary layer over a flat plate, as well

Table 2

Summary of the turbulent boundary layer properties at streamwise location of $x = 1.8 \text{ m}$ obtained from PIV measurements.

	Flat surface	Riblet coating
U_e (m/s)	3.8	3.8
δ_{99} (mm)	26.4	23.2
θ (mm)	2.5	2.1
u_τ (m/s)	0.14	0.1385
$Re_\tau = U_e L/\nu$	7.207×10^6	
$Re_\tau = u_\tau \delta_{99}/\nu$	3847	3344
$Re_\theta = U_e \theta/\nu$	9890	8300
$s^+ = u_\tau s/\nu$	–	13.2

as the riblet coating. A literature overview is presented in Table 1 to emphasize the difference of current research from other experimental investigations over riblet surfaces by means of riblet spacing and the Reynolds number. Throughout the listed studies, current work focuses on comparably small riblet spacing and high Reynolds number flow (see Table 2).

2. Facility and technique

2.1. Experimental set-up and material

Experiments were performed in a closed loop water tunnel (Fig. 2a) at the Ship Hydromechanics group of the TU Delft. Dimensions of the test section are $(2 \times 0.3 \times 0.35) \text{ m}^3$ in length, width, and height, respectively. The boundary layer under consideration develops over the top wall of the tunnel at (nearly) zero pressure gradient conditions due to a sloping opposite wall. The flow speed can be increased up to 7 m/s, which enables to study realistic flow conditions for surface modification with riblet, compliant coatings, etc. More details for the tunnel can be found in Zverkhovskiy [24]. A zigzag strip was placed at the entrance of the tunnel to ensure the boundary layer flow is turbulent [25].

The coating used in this study has a trapezoidal riblet shape where the spacing between the riblet tips, s , is $92 \mu\text{m}$. The coating is manufactured from a commercial fouling release product (Intersleek® 1100SR, International Paint / AkzoNobel) whose composition has been modified by increasing the overall volume solids from 72% to 96% to enable preparation of a surface with defect free, high fidelity, trapezoidal riblet shapes (see Fig. 1). Further detail of the coating, including SEM (scanning electron microscope) pictures, can be found in Benschop et al. [19], their Fig. 2b.

The virtual origin of the coating was calculated according to Bechert and Bartenwerfer [26]; i.e., the origin of the velocity profile lies below the riblet tips where the related distance is described as the protrusion height which cannot exceed 22% of the lateral riblet spacing. The coating was applied to a flat plate of length $L = 2 \text{ m}$ and width

Table 1

Literature overview of relevant researches on drag reducing riblet surfaces.

Experiments on continuous riblet surfaces	Reynolds number	Experimental Facility	Type of wall-bounded turbulence	Riblet spacing (mm) & s^+ interval	Experimental Technique
Vukoslavcevic et al. [21]	$Re_\theta = 1000$	Wind tunnel	Flat plate	$s = 10$ & $s^+ = 35$	Hot wire
Park & Wallace [14]	$Re_\theta = 1200, 2100, 2500$	Wind tunnel	Flat plate	$s = 10$ & $s^+ = 18, 28, 46$	Hot-wire
Bechert et al. [9]	$10,000 \leq Re_{ch} \leq 33000$	Oil channel	Channel flow	Effect of riblet spacing was investigated	Shear stress balance
Lee & Lee [13]	$Re_\theta = 2340, Re_\theta = 4950$	Wind tunnel	Flat plate	$s = 3$ & $s^+ = 25.2, 40.6$	PIV and PTV
Lee & Choi, [16]	$Re_\theta = 3790$	Wind tunnel	Flat plate	$s = 0.3$ & $s^+ = 10.4$	PIV
Li et al. [22]	$Re_\theta = 1200, Re_\theta = 2080$	Wind tunnel	Flat plate	$s = 0.75$ & $s^+ = 24, 45$	PIV and μPIV
Hou et al. [18]	$Re_\theta = 2384$	Water channel	Channel flow	$s = 0.75$ & $s^+ = 11$	2D-3D PIV, PTV, μPTV and tomo-PIV
Rowin et al. [23]	$Re_{ch} = 4360$	Water channel	Channel flow	$s = 0.75$ & $s^+ = 8.6, 17.3, \text{ and } 34.6$	Planar PIV
Benschop et al. [19]	$10^4 \leq Re_s \leq 10^5$	Taylor- Couette set-up	Taylor- Couette flow	$s = 0.092$ & $1 \leq s^+ \leq 20$	Torque-meter
Current work	$Re_\theta = 9890$	Water tunnel	Flat plate	$s = 0.092$ & $s^+ = 13.4$	Force balance, Stereo-PIV

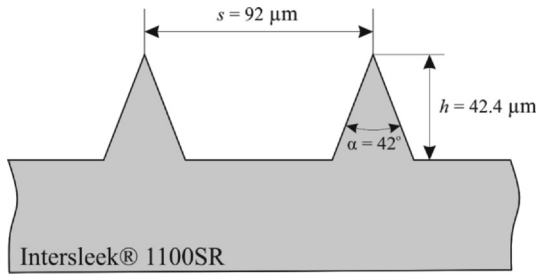


Fig. 1. Schematic presentation of the riblet shape with geometric details. For more details, see Benschop et al. [19].

$w = 0.298$ m, which were mounted in the test section replacing the top wall. The results for the riblet coated plate were compared with those for a hydraulically smooth flat plate in order to examine the drag reduction mechanism. The drag reducing range, determined with respect to dimensionless riblet spacing, $s^+ = su_\tau/\nu$ (where $\nu = 0.949 \times 10^{-6}$ m²/s) was $2 < s^+ < 14$. The friction velocity, u_τ , were evaluated from force measurements using $u_\tau = \sqrt{\tau_w/\rho}$ where τ_w is the averaged wall shear stress (N/m²) on the plate and ρ is the water density in kg/m³.

2.2. Force measurement

The force measurements were performed using an external moving frame that is specially designed for having one degree of freedom in the direction of the free stream flow. Any plate with specific dimensions can be attached on this moving frame and carried by two leaf springs enabling direct measurement of the drag force, F_D . The test plate was precisely positioned using alignment screws on fixed frame, resulting in an angle of attack to the flow of $O(0.01^\circ)$. A picture is presented in Fig. 2a showing the location of force balance, including a pulley mechanism for calibration. The force sensor (ZEMIC L6D Class-3, with a precision of $\pm 0.023\%$ of the full-scale) used in the experiments was calibrated using this pulley mechanism applying various weights according to the measurement range. The sampling frequency of the force sensor was 1 kHz, and the signals were analyzed by calculating the sample mean for the data recorded. A cross-view of the set-up is presented in Fig. 2b to show the details of the drag measurement mechanism. The leaf springs are attached to a fixed frame on the top, and the test plates on the bottom. There exist 1 mm gaps at both sides of the plate, which may cause water leaks and hence the error in the measurement. In order to prevent water leaks, thin, flexible strips were

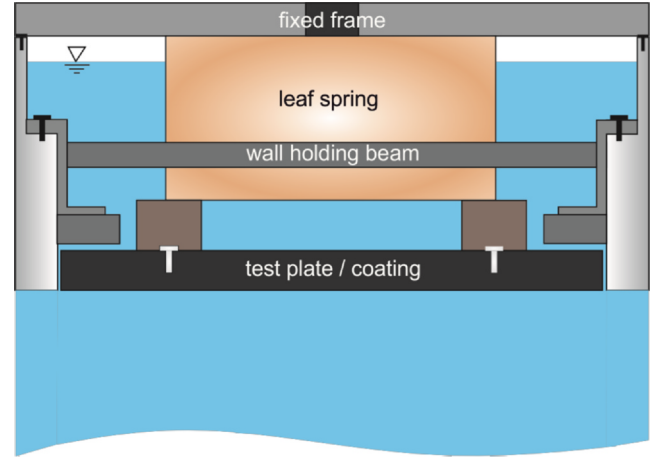


Fig. 2b. Schematic presentation of the cross-view of experimental set-up.

attached, satisfying the attached flow on the test plate.

The non-dimensional drag coefficient is defined as,

$$C_D = 2F_d/\rho U_e^2 A \quad (2.1)$$

where A is the surface area of the plate, U_e is the free-stream velocity of the flow, and ρ is the density (kg/m³) calculated at the average temperature during the measurements. To validate the results with available theory, the drag coefficient was also calculated using the relationship:

$$C_{D,theo} = 0.031/Re_L^{1/7}, \text{ where } Re_L = U_e L/\nu \quad (2.2)$$

(ν is the kinematic viscosity in m²/s) derived by one-seventh power law [27]. The results are presented in Fig. 3 for a wide range of Reynolds number. It is clear that the measurements for low Re_L demonstrate strong deviations from the theoretical curve according to non-turbulent transition around $Re \approx 10^6$; therefore $Re_L > 2 \times 10^6$ looks to be reliable for processing and will be used for further analysis. Water level of the tunnel was kept constant as $h_w = 0.3$ m for all velocities to eliminate possible bias caused by the water height. Since the force measurements on the test plate started with $U_\infty = 0.4$ m/s, measurements were corrected by fitting a second-order polynomial to the force data with respect to velocity, and then an offset (about 1% of the measured force) was applied to the data, considering zero force at zero velocity. For $Re_L > 2 \times 10^6$, the uncertainty in the measurements was estimated to be less than 0.1% at 95% confidence level.

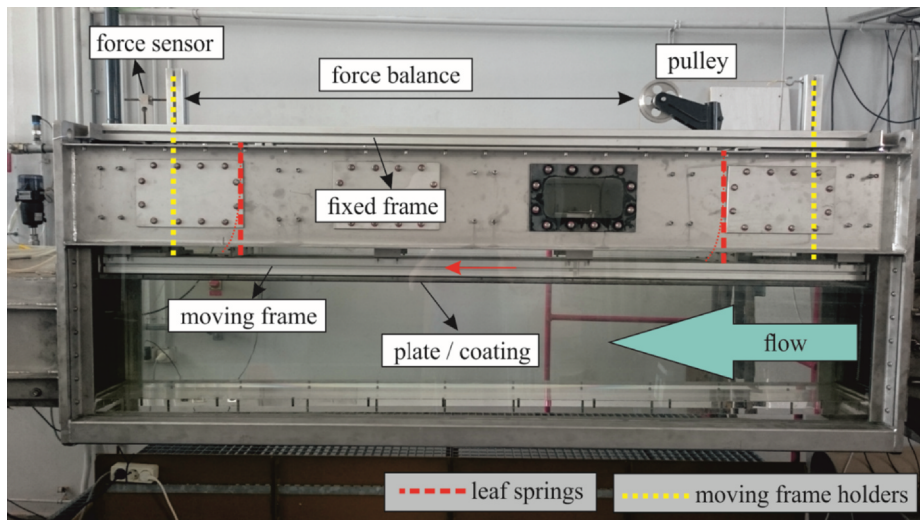


Fig. 2a. General view of the tunnel and force measurement system.

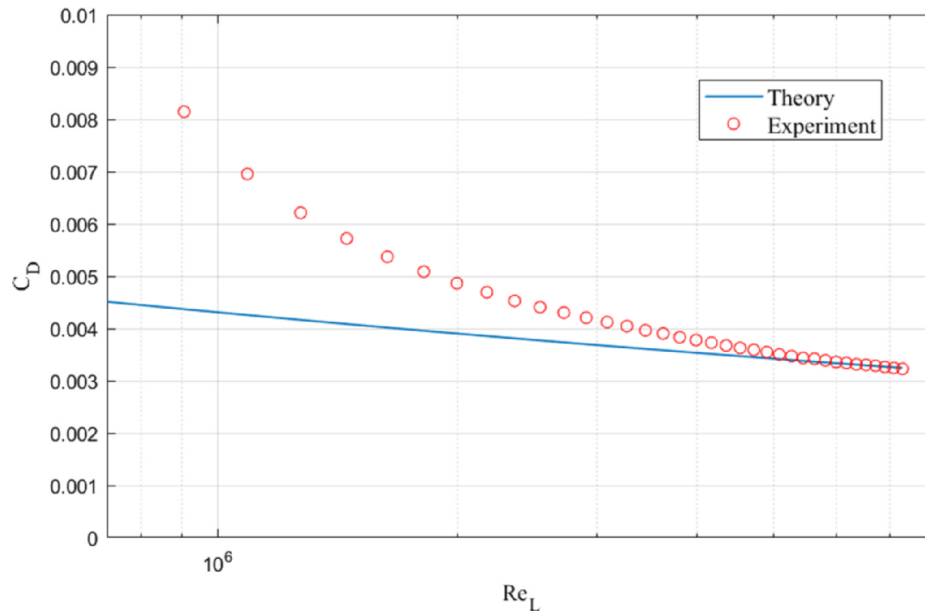


Fig. 3. Drag coefficients calculated by experiments and theory (one-seventh power law).

2.3. Velocity measurement

All three components of the velocity were measured in a cross-stream plane using stereo-PIV as shown in Fig. 4. The experiments were performed considering the case with highest drag reduction ($s^+ = 13.2$). Two high-speed CMOS cameras (pco.dimax, 4 M, 2016×2016 pix resolution, 12-bit dynamic range, 1279 fps) at 45° viewing angles were used to capture the particle images (Fig. 4). The cameras were mounted with 105 mm Nikon lenses at $f/5.6$ satisfying the Scheimpflug condition [28]. Furthermore, water filled prisms were used to minimize the optical deformation of the images due to refractive changes at air-water interface. The flow was seeded with neutrally buoyant hollow glass spheres with $10 \mu\text{m}$ diameter. A double-

pulsed Nd:YLF laser having 527 nm wavelength and 10 mJ/pulse output with a repetition rate of 10 Hz was used for the illumination. The sheet was formed with two lenses and directed such as to obtain forward scattering in which the tracer particles scatter more light according to Mie theory [29]. The thickness of the laser sheet and time between images were adjusted to 1 mm and 25 μs , respectively, ensuring that there is only limited out of plane motion. The thin light sheet perpendicular to the mean flow resulted in a low signal-to-noise ratio [31]. The calibration was done using a plexiglass plate with “+” signs printed in increments of 5 mm. A traversing mechanism was used for displacing the plate in steps of 0.5 mm to calibrate the stereo PIV system. Furthermore, the self-calibration procedure was performed [30] in order to minimize the errors caused by misregistration [31]. 1570 images were captured and used for self-calibration for all data sets. Davis v.8.0 was used for the calibration and cross-correlation analysis. A final interrogation window size of 24×24 pixels was employed with a 50% overlap. The final field of view has dimensions of $(y, z) = (41.8 \times 54.2) \text{ mm}^2$ corresponding to an average magnification of $M = 0.41$, yielding a resolution of 37.6 px/mm in the object plane. The spatial resolution of the measurements was, therefore, $\Delta y = \Delta z = 0.3188 \text{ mm}$. The number of spurious vectors was less than 5%. The correlation noise of the y - and z -components of the vector field were $\sigma_{corr} \approx 0.1 \text{ px}$, in agreement with Westerweel [32]. Hence, considering the maximum value of the free-stream flow, the uncertainty in the velocity was estimated to be less than 2%. The velocity gradients, hence the vorticity were estimated by means of flow circulation by first applying Gaussian kernel to attenuate the noise level [33]. According to Foucaut and Stanislas [34], the uncertainty in the vorticity estimation was calculated to be less than 5%.

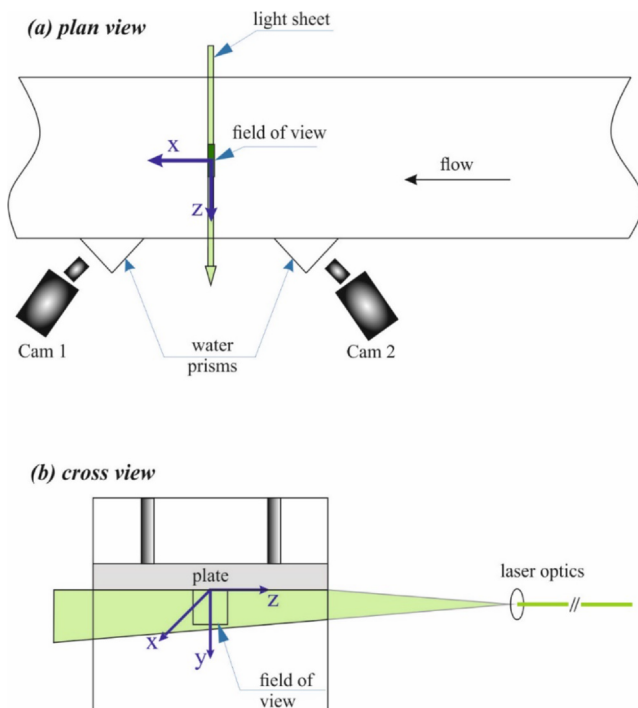


Fig. 4. Schematic presentation of stereo-PIV configuration.

2.4. Two-point correlations

In order to quantify the statistical behavior of turbulent structures within the available flow domain, two-point spatial correlations of the fluctuating velocity components are widely utilized [35]. For example, two-point spatial correlation of the streamwise velocity fluctuations, u , are used to gain information about the hairpin packets [36] in the log region. For the available flow field and coordinate system, it is defined as:

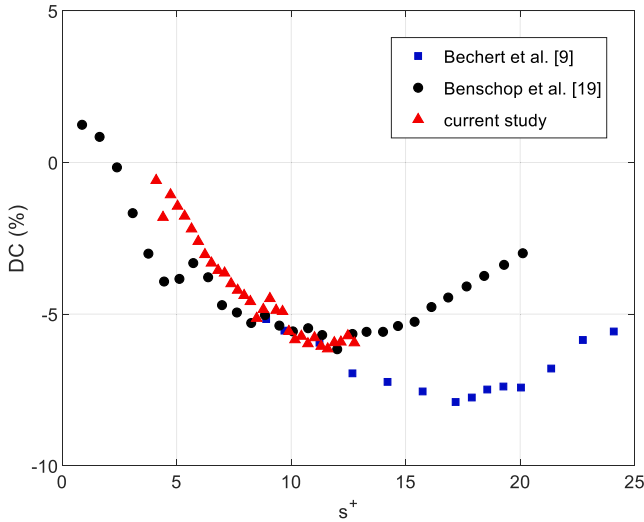


Fig. 5. Drag reducing effect of the riblet coating, together with Bechert et al. [9] and Benschop et al. [19].

$$R_{uu}(y, z, \Delta y, \Delta z) = \frac{\langle u(y, z)u(y + \Delta y, z + \Delta z) \rangle}{\sigma_u^2} \quad (2.3)$$

where σ_u is the standard deviation of streamwise velocity fluctuations and, Δy and Δz are the wall-normal and spanwise separation, respectively between the data points in measurement plane. The brackets represent the ensemble average of the data over the recorded image frames. The PIV velocity field has inhomogeneous velocity components since the current study focuses on the cross-stream plane where the wall and riblets introduce non-uniformity. Thereby, equation (2.3) was directly computed at the selected reference points, (y, z) .

3. Results

The drag reducing effect of coating is expressed as a drag change in percentage calculated by $DC = 100 \times (C_D^{riblet} - C_D^{flat})/C_D^{flat}$, which is presented and compared with Bechert et al. [9] and Benschop et al. [19] in Fig. 5. Here, the low Reynolds number data of current study ($Re < 2 \times 10^6$) are not included due to inaccurate drag measurements of non-turbulent transition ($Re \approx 10^6$), which was shown in Fig. 3. It can be seen that the drag reduction behavior is identical to that observed by Bechert et al. [9], and a maximum reduction of 5.9% is obtained. The results are also in good agreement with the Taylor-Couette measurements of the same riblet coating presented in Benschop et al. [19], albeit their flow geometry is different. The agreement between the results of current study and Benschop et al. [19] shows that less time consuming and lower-cost Taylor-Couette flow measurements may be used as an alternative to turbulent boundary layer measurements over a flat plate.

Once the drag reducing effect of riblet coatings has been verified, PIV measurements were performed at the speed corresponding to the highest drag reduction, i.e. $s^+ = 13.2$. In Fig. 6, semi log profiles of mean velocity as a function of wall-normal distance normalized by local friction velocities are presented and compared with the generalized formula of Spalding [37] and hot-wire data of Carlier & Stanislas [38]. As evident from the figure, the mean velocity profile of the flat surface fits well with the literature [37] showing a visible logarithmic region in the overlap layer evaluated using von Kármán and integral constants as $k = 0.4$ and $B = 5$, respectively. The mean velocity profile for the flat surface also agrees well with results from Carlier & Stanislas [38], however with slight deviations. The discrepancy of data points close to the wall is due to the limited spatial resolution of the PIV measurements. As compared with the flat surface, an upward shift is obtained for the coating, which is associated with an apparent thickening of the

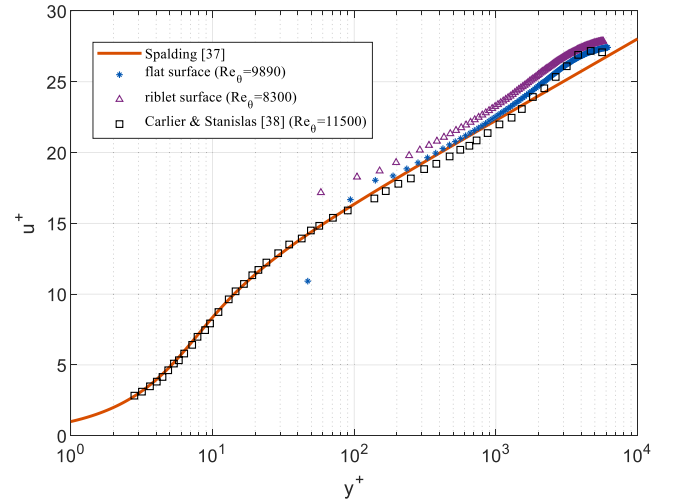


Fig. 6. Dimensionless mean velocity profile for flat and riblet surfaces with Spalding's fit [37] and hotwire data of Carlier & Stanislas [38].

viscous sublayer [10] resulting in a decreased friction velocity and skin friction. This upward shift in the velocity profile has been observed frequently for drag reducing riblets [13,17,18,39,40] and described as a possible consequence of modified near-wall turbulent structures due to the energy balance between reduced turbulent kinetic energy production and viscous dissipation [41].

The effect of the riblets is to reduce the velocity fluctuations especially in the streamwise and wall-normal directions as reported previously [16–18]. This indicates a decreased momentum transfer and turbulent mixing in the turbulent boundary layer. The present results shown in Fig. 7 agree well with those earlier findings; here the free-stream and friction velocities used for normalization were considered individually for flat and riblet surfaces. The turbulent kinetic energy and Reynolds shear stress profiles for the riblet surface are slightly below the respective profiles for the flat surface. The profiles match with each other outside of the boundary layer ($y > \delta$). Discrepancies in turbulent kinetic energy and Reynolds shear stress tend to get smaller when friction velocity is used for normalization; however, the riblet profile is still below the profile for the flat plate. Physically, decreased statistics of fluctuating velocity is key evidence for reduced turbulent mixing and less efficient transport of high-momentum outer fluid toward the surface. Besides, the lower Reynolds shear stress implies that sweep and ejection motions, which significantly contribute to the skin friction, are attenuated.

One of the main characteristics of turbulence are vortical structures, hence the effect of riblet surface on streamwise vorticity fluctuations, $\langle \omega_x^+ \rangle = \langle \sqrt{(\omega_x^+)^2} \rangle > v/u_\tau$ is presented in Fig. 8. Related research has revealed that up to a certain wall-normal distance, i.e. $y^+ = 15$ [18] or $y^+ = 130$ [42], the vorticity fluctuations are reduced above riblets compared to the flat surface. These studies reported that $\langle \omega_x^+ \rangle$ tends to have the same magnitude over flat and riblet surfaces beyond the mentioned wall-normal distances. However, these investigations have considered channel flow, and therefore they have limited data for larger wall-normal distances. The present vorticity profiles (Fig. 8) are in good agreement with these earlier works covering the near wall region [10,18,42], while presenting additional information for the whole boundary layer. The vorticity fluctuations seem to be slightly lower over riblets up to $y^+ = 500$ and at this point the values are identical for both surfaces. However, an obvious increase in the deviation occurs for $y^+ \geq 500$. Compared with the flat surface, a reduction of about 6% occurs in vorticity fluctuations within the log layer of the riblet surface.

The two-point correlations give information about the typical size and strength of turbulent flow features. Fig. 9 presents the auto correlation of the streamwise velocity fluctuations which can be used to

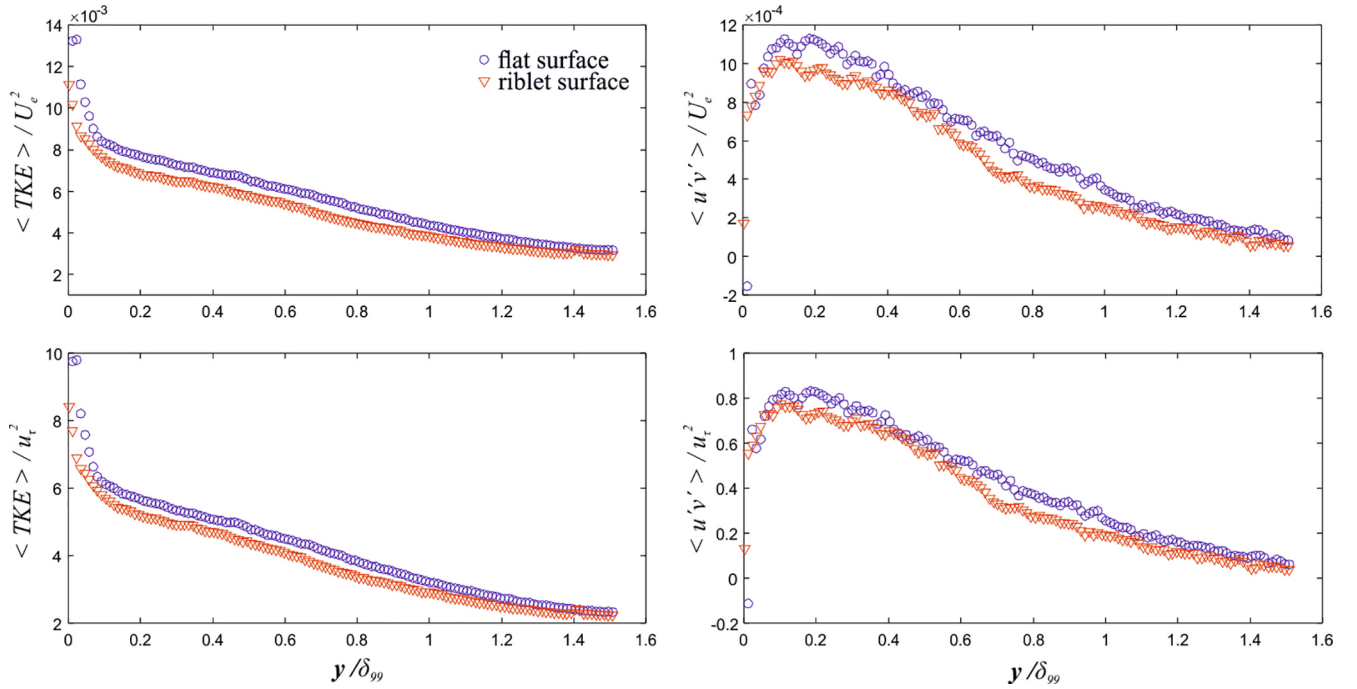


Fig. 7. Comparison of time-averaged Turbulent Kinetic Energy, $\langle TKE \rangle$ and Reynolds Shear Stress, $\langle u'v' \rangle$ normalized by free-stream velocity, U_e (top) and local friction velocity, u_τ (bottom).

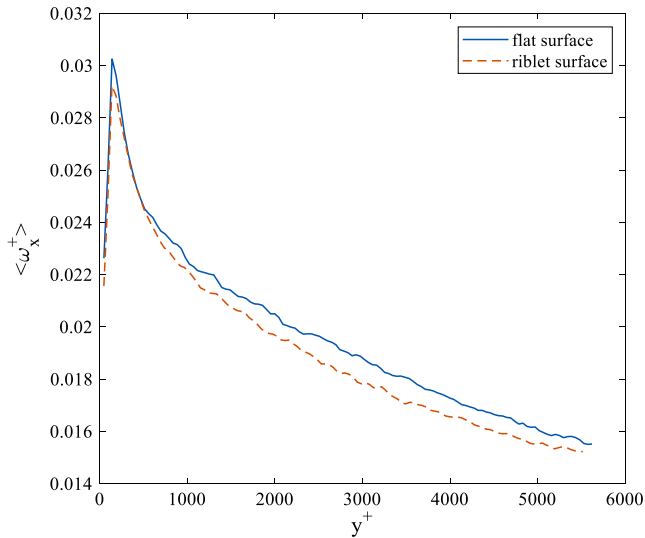


Fig. 8. Streamwise root mean square vorticity fluctuation normalized using local friction velocities of flat and riblet surfaces.

characterize the high and low speed regions. The flow field was cropped, and only positive correlation contours are presented to make it clear for comparison. Firstly, the correlations clearly show the growth with increasing the wall-normal reference position, which is consistent with Townsend's attached eddy hypothesis in which the size of an eddy along the spanwise and wall-normal directions is proportional to its distance from the wall [43]. Next, the structure size and shape over riblet and flat surfaces look almost identical at $y^+ = 232$. However, the structure size over riblet surface tends to decrease in width. This tendency yields an absolute difference in structure size where it becomes narrower over the riblet surface compared to the smooth wall at wall normal distances of $y^+ = 511$ and $y^+ = 976$. The decrease in vorticity fluctuations depicted in Fig. 8 for $y^+ \geq 500$ could also be associated and in accordance with the two-point correlations obtained at $y^+ = 511$. Therefore it can be concluded that the riblets are effective on

decreasing the size of turbulent eddies within the log region of a turbulent boundary layer.

The quadrant analysis applied to Reynolds shear stress is a useful tool to evaluate information on the sign of velocity fluctuations, hence the special events occurring in a turbulent boundary layer. The quadrants are related to velocity information according to: Q1($u > 0, v > 0$), Q2($u < 0, v > 0$), Q3($u < 0, v < 0$), Q4($u > 0, v < 0$) which are also known as sweep (Q4)-ejection (Q2) motions and inward (Q1)-outward (Q3) interactions [44]. The products of the fluctuations classify the events. Fig. 10 presents the conditional averaged and normalized Reynolds shear stress distributions in wall-normal direction for all quadrants, agreeing well with relevant literature [45]. The gradient-type motions; Q2 and Q4 events have the most significant contribution to Reynolds shear stress [46], i.e. the turbulence production. However, in general, Q2 has a larger contribution compared to Q4 [45], since the obtained data is in the log layer. Moreover, all quadrants have slightly decreased magnitudes over riblet surface in correspondence with related studies [10,18,42]. Inherently, the deviation in magnitudes for Q2 and Q4 events is larger compared with Q1 and Q4, and this deviation is valid throughout the outer region. Therefore it should be noted that the attenuation effect of riblet surface on turbulence production lasts even for the wake region.

4. Conclusions

In this study, the difference between flow structures over flat and riblet surfaces in the cross-stream plane is analyzed and interpreted in order to understand the underlying mechanism of drag reduction. In this sense, the Reynolds number considered was much higher than before, together with a comparably small-sized riblet spacing, both corresponding to the actual flow conditions encountered in most industrial applications. The drag reducing effect of a trapezoidal riblet coating is first verified by force measurements agreeing well with the literature [9,19]. According to the agreement in force measurements of Benschop et al. [19], it was revealed that the Taylor-Couette flow facility may be used as an alternative set-up over more time-consuming and costly measurements over a flat surface.

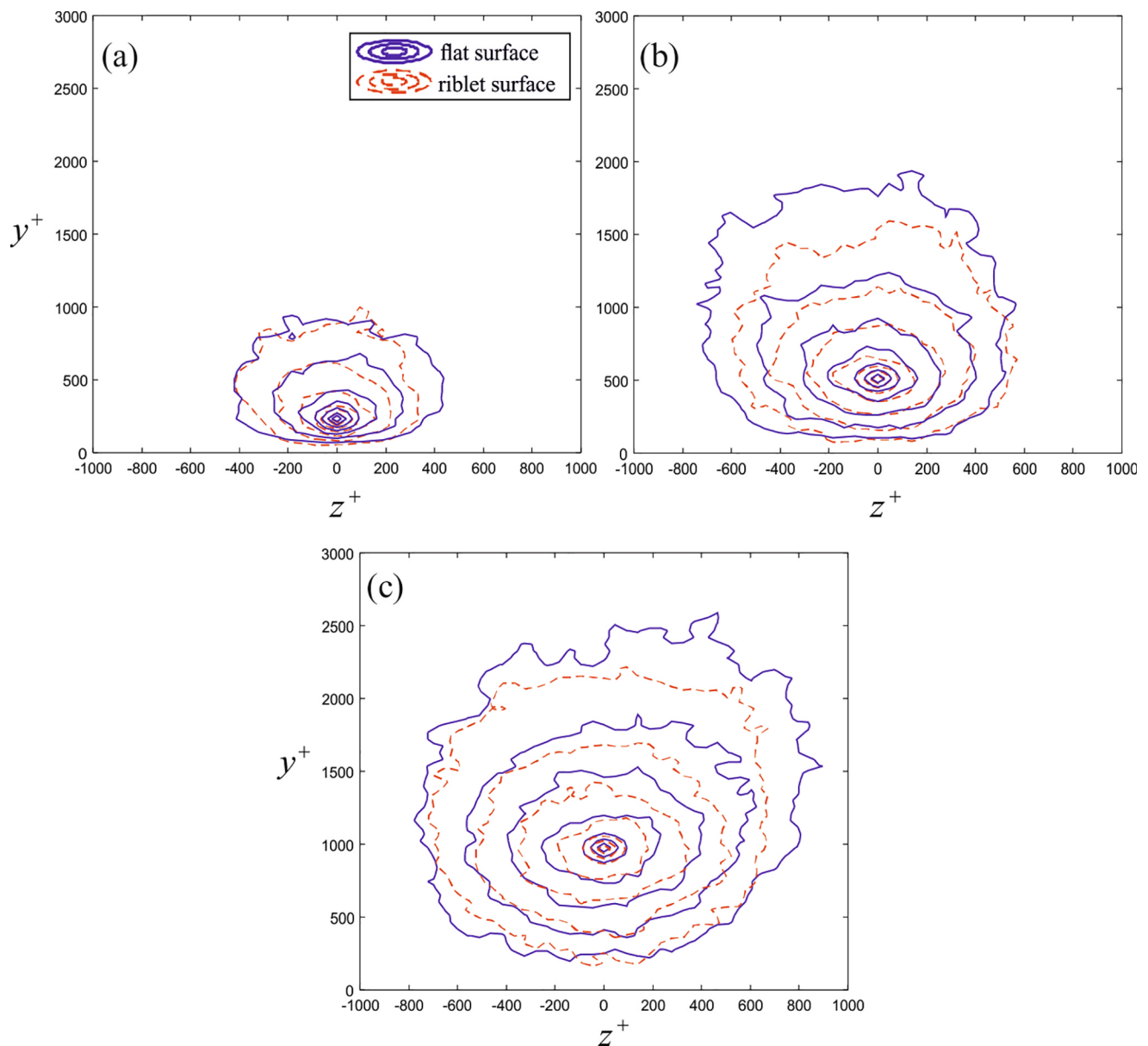


Fig. 9. The correlation of streamwise velocity fluctuations, R_{uu} of flat and riblet surfaces normalized with local friction velocities at wall-normal positions of (a) $y^+ = 232$, (b) $y^+ = 511$ and (c) $y^+ = 976$. The contour levels range from 0.3 to 1 with a spacing of 0.1.

Next, the stereo-PIV measurements were performed at the maximum drag reducing case. The data was post-processed with a focus on time-averaged turbulent statistics. For the mean velocity profile, an upward shift was obtained for the riblet surface due to the decrease in friction velocity. Time-averaged Reynolds shear stress and turbulent kinetic energy over riblet surface were attenuated compared with the flat surface as an indication of reduced turbulent transport towards the wall. This is further elaborated through time-averaged vorticity fluctuations, two-point spatial correlations, and quadrant analysis.

Over the riblet surface, it was found that the evaluated vorticity fluctuations were slightly reduced close to the wall, however, for $y^+ \geq 500$, the reduction found was obtained greater, i.e., a maximum of 6%. The special events, especially the sweep and ejection within the boundary layer, is known to be the primary source of the transport of Reynolds shear stresses. It was evaluated that over riblets the magnitudes of sweep and ejection events were slightly dropped throughout the boundary layer. Furthermore, two-point spatial correlations aided to further understanding providing signatures of hairpin vortices. Two-point correlations of streamwise velocity fluctuations showed that the

turbulent structure over the riblet surface is smaller for $y^+ \geq 511$ following the results of vorticity fluctuations. It was concluded that this is an indication of possible suppression on quasi-streamwise vortices and decrease in transport of vorticity, hence the turbulence production.

5. Compliance with Ethical Standards

Funding

The manufacturing of riblet coating used in this research has received funding from the European Union Seventh Framework Programme in the SEAFRONT project [grant agreement number 614034]. The first author is funded by The Scientific and Technological Research Council of Turkey (TUBITAK) under application number of 1059B191600985.

CRedit authorship contribution statement

G.M. Ozkan: Conceptualization, Formal analysis, Investigation,

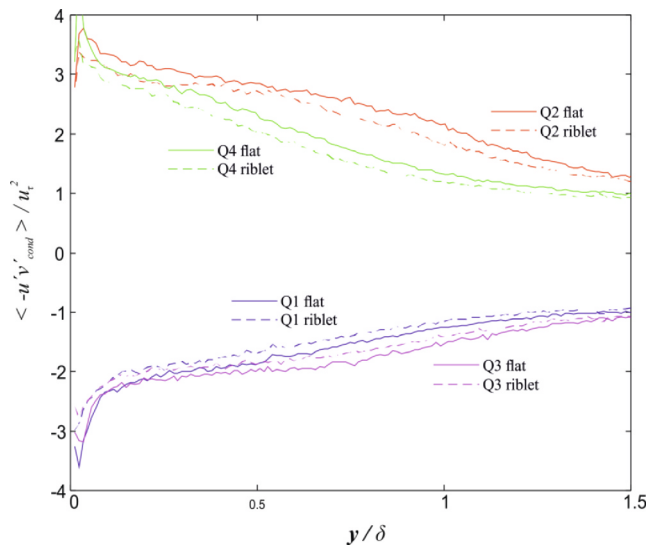


Fig. 10. Conditionally averaged Reynolds shear stresses normalized with local friction velocities for flat and riblet surfaces.

Writing - original draft, Visualization, Data curation. **G.E. Elsinga:** Writing - review & editing, Supervision, Methodology. **W.-P. Breugem:** Writing - review & editing, Project administration, Funding acquisition. **D. Stübing:** Resources, Methodology. **K.J. Reynolds:** Resources, Methodology. **J. Westerweel:** Supervision, Conceptualization, Writing - review & editing, Methodology.

Declaration of Competing Interest

The authors declare that they have no known competing financial interests or personal relationships that could have appeared to influence the work reported in this paper.

References

- [1] L. Prandtl, Über Flüssigkeitsbewegung bei sehr kleiner Reibung, in: Proc. Third Int. Math. Cong., Heidelberg, Germany, 1904, pp. 484–491.
- [2] M. Gad-el-Hak, Flow Control: Active, Passive and Reactive Flow Management, Cambridge University Press, 2000.
- [3] M. Perlin, D.R. Dowling, S. Ceccio, Freeman scholar review: passive and active skin-friction drag reduction in turbulent boundary layers, *J. Fluids Eng.-Trans. ASME* 138 (9) (2016).
- [4] D.M. Bushnell, K.J. Moore, Drag reduction in nature, *Annu. Rev. Fluid Mech.* 23 (1991) 65–79.
- [5] D.W. Bechert, M. Bruse, W. Hage, R. Meyer, Fluid mechanics of biological surfaces and their technological application, *Naturwissenschaften* 87 (2000) 157–171.
- [6] B. Bhushan, Biomimetics: lessons from nature - an overview, *Philos. Trans. Roy. Soc. A-Math. Phys. Eng. Sci.* 367 (1893) (2009) 1445–1486.
- [7] M.J. Walsh, Riblets as viscous drag reduction technique, *AIAA J.* 21 (1983) 485–486.
- [8] P. Luchini, F. Manzo, A. Pozzi, Resistance of a grooved surface to parallel flow and cross-flow, *J. Fluid Mech.* 228 (1991) 87–109.
- [9] D.W. Bechert, M. Bruse, W. Hage, J.G.T. Van der Hoeven, G. Hoppe, Experiments on drag-reducing surfaces and their optimization with an adjustable geometry, *J. Fluid Mech.* 338 (1997) 59–87.
- [10] H. Choi, P. Moin, J. Kim, Direct numerical simulation of turbulent flow over riblets, *J. Fluid Mech.* 255 (1993) 503–539.
- [11] D. Goldstein, R. Handler, L. Sirovich, Direct numerical-simulation of turbulent-flow over a modeled Riblet covered surface, *J. Fluid Mech.* 302 (1995) 333–376.

- [12] B. Dean, B. Bhushan, Shark-skin surfaces for fluid-drag reduction in turbulent flow: a review, *Philos. Trans. Roy. Soc.* 368 (2010) 4775–4806.
- [13] S.J. Lee, S.H. Lee, Flow field analysis of a turbulent boundary layer over a riblet surface, *Exp. Fluids* 30 (2) (2001) 153–166.
- [14] S.R. Park, J.M. Wallace, Flow alteration and drag reduction by riblets in a turbulent boundary-layer, *AIAA J.* 32 (1) (1994) 31–38.
- [15] J.J. Wang, et al., Experimental study on the turbulent boundary layer flow over riblets surface, *Fluid Dyn. Res.* 27 (4) (2000) 217–229.
- [16] S.J. Lee, Y.S. Choi, Decrement of spanwise vortices by a drag-reducing riblet surface, *J. Turbul.* 9 (23) (2008) 1–15.
- [17] A. Boomsma, F. Sotiropoulos, Direct numerical simulation of sharkskin denticles in turbulent channel flow, *Phys. Fluids* 28 (3) (2016).
- [18] J.F. Hou, et al., Three-dimensional measurement of turbulent flow over a riblet surface, *Exp. Therm Fluid Sci.* 85 (2017) 229–239.
- [19] H.O.G. Benschop, A.J. Guerin, A. Brinkmann, M.L. Dale, A.A. Finnie, W.-P. Breugem, A.S. Clare, Stübing, D.C. Price, K.J. Reynolds, Drag-reducing riblets with fouling-release properties: development and testing, *Biofouling* 34 (5) (2018) 532–544.
- [20] A.J. Smits, I. Marusic, Wall-bounded turbulence, *Phys. Today* 66 (9) (2013) 25.
- [21] P. Vukoslavcevic, J.M. Wallace, J.-L. Balint, Viscous drag reduction using streamwise-aligned riblets, *AIAA J. Tech. Notes* 30 (1992) 4.
- [22] W. Li, W. Jessen, D. Roggenkampa, M. Klaas, W. Silex, M. Schiek, W. Schröder, Turbulent drag reduction by spanwise traveling ribbed surface waves, *Eur. J. Mech. B/Fluids* 53 (2015) 101–112.
- [23] W.A. Rowin, J. Hou, S. Ghaemi, Turbulent channel flow over riblets with superhydrophobic coating, *Exp. Therm Fluid Sci.* 94 (2018) 192–204.
- [24] O. Zverkhovskiy, Ship Drag Reduction by Air Cavities, Ph.D. Thesis, TU Delft, 2014.
- [25] G. Elsinga, J. Westerweel, Tomographic-PIV measurement of the flow around a zigzag boundary layer trip, *Exp. Fluids* 52 (4) (2012) 865–876.
- [26] D.W. Bechert, M. Bartenwerfer, The viscous flow on surfaces with longitudinal ribs, *J. Fluid Mech.* 206 (1989) 105–129.
- [27] M.F. White, Fluid Mechanics, McGraw Hill, 2003.
- [28] A. Prasad, Stereoscopic particle image velocimetry, *Exp. Fluids* 29 (2000) 103–116.
- [29] M. Born, E. Wolf, Principles of Optics, Pergamon Press, Oxford, 1975.
- [30] B. Wieneke, Stereo-PIV using self-calibration on particle images, *Exp. Fluids* 39 (2005) 267–280.
- [31] V. Doorne, J. Westerweel, Measurement of laminar, transitional and turbulent pipe flow using Stereoscopic-PIV, *Exp. Fluids* 42 (2007) 259–279.
- [32] J. Westerweel, Theoretical analysis of the measurement precision in particle image velocimetry, *Exp. Fluids* 29 (Supplementary) (2000) S3–S12.
- [33] C.C. Landreth, R.J. Adrian, Impingement of a Reynolds number turbulent circular jet onto flat plate at normal incidence, *Exp. Fluids* 9 (1990) 74–84.
- [34] J.M. Foucaut, M. Stanislas, Some considerations on the accuracy and frequency response of some derivative filters applied to particle image velocimetry vector fields, *Meas. Sci. Technol.* 13 (2002) 1058–1071.
- [35] J.A. Sillero, J. Jiménez, R.D. Moser, Two-point statistics for turbulent boundary layers and channels at Reynolds numbers up to $\delta^+ \approx 2000$, *Phys. Fluids* 26 (2014) 105109.
- [36] R.J. Adrian, Hairpin vortex organization in wall turbulence, *Phys. Fluids* 19 (2007) 041301.
- [37] D.B. Spalding, A single formula for the law of the wall, *J. Appl. Mech.* 28 (1961) 455–457.
- [38] J. Carlier, M. Stanislas, Experimental study of eddy structures in a turbulent boundary layer using particle image velocimetry, *J. Fluid Mech.* 535 (2005) 143–188.
- [39] O.A. El-Samni, H.H. Chun, H.S. Yoon, Drag reduction of turbulent flow over thin rectangular riblets, *Int. J. Eng. Sci.* 45 (2007) 436–454.
- [40] A. Rastegari, R. Akhavan, The common mechanism of turbulent skin-friction drag reduction with superhydrophobic longitudinal microgrooves and riblets, *J. Fluid Mech.* 838 (2018) 68–104.
- [41] E. Coustols, Riblets: Main known and unknown features, in: K.-S. Choi, K.K. Prasad, T.V. Truong (eds.), *Emerging Techniques in Drag Reduction*, Mechanical Engineering Publications Limited, Bury St. Edmunds, London, UK, 1995, pp. 3–43.
- [42] M. Sasamori, H. Mamori, K. Iwamoto, A. Murata, Experimental study on drag reduction effect due to sinusoidal riblets in turbulent channel flow, *Exp. Fluids* 55 (2014) 1828.
- [43] A.A. Townsend, *The Structure of Turbulent Shear Flow*, second ed., Cambridge University Press, Cambridge, 1976.
- [44] J.M. Wallace, R.S. Brodkey, H. Eckelmann, The wall region in turbulent shear flow, *J. Fluid Mech.* 54 (1972) 39–48.
- [45] J.M. Wallace, Quadrant analysis in turbulence research: History and evolution, *Annu. Rev. Fluid Mech.* 48 (2016) 131–158.
- [46] W.W. Willmarth, S.S. Lu, Structure of the Reynolds stress near the wall, *J. Fluid Mech.* 55 (1972) 65–92.